Journal of Geography and Cartography 2025, 8(2), 11424.
https://doi.org/10.24294/jgc11424

Article

Evaluation of classification methods and algorithms for mapping land cover change in a mining locality in Southeastern D.R. Congo

John Tshibangu Wa Ilunga[1,*], Yves Katumbwe Lumbu[2], Olivier Ngoie Inabanza[1], Joseph Mukalay Muamba[1,3], Junior Muyumba Munganga[1], Urcel Kalenga Tshingomba[1], Catherine Nsiami Mabiala[1]

[1] Faculty of Sciences, University of Lubumbashi, Lubumbashi 1825, Democratic Republic of the Congo
[2] Independent researcher in remote sensing applied to the environment, Lubumbashi 7010, Democratic Republic of the Congo
[3] Faculty of Agronomic Sciences, University of Lubumbashi, Lubumbashi 1825, Democratic Republic of the Congo
*** Corresponding author:** John Tshibangu Wa Ilunga, johntshiwil@gmail.com

CITATION

Tshibangu WIJ, Katumbwe LY, Ngoie IO, et al. Evaluation of classification methods and algorithms for mapping land cover change in a mining locality in Southeastern D.R. Congo. Journal of Geography and Cartography. 2025; 8(2): 11424. https://doi.org/10.24294/jgc11424

ARTICLE INFO

Received: 27 January 2025
Accepted: 7 March 2025
Available online: 8 April 2025

Abstract: To study the environment of the Kipushi mining locality (LMK), the evolution of its landscape was observed using Landsat images from 2000 to 2020. The evolution of the landscape was generally modified by the unplanned expansion of human settlements, agricultural areas, associated with the increase in firewood collection, carbonization, and exploitation of quarry materials. The problem is that this area has never benefited from change detection studies and the LMK area is very heterogeneous. The objective of the study is to evaluate the performance of classification algorithms and apply change detection to highlight the degradation of the LMK. The first approach concerned the classifications based on the stacking of the analyzed Landsat image bands of 2000 and 2020. And the second method performed the classifications on neo-images derived from concatenations of the spectral indices: Normalized Difference Vegetation Index (NDVI), Normalized Difference Building Index (NDBI) and Normalized Difference Water Index (NDWI). In both cases, the study comparatively examined the performance of five variants of classification algorithms, namely, Maximum Likelihood (ML), Minimum Distance (MD), Neural Network (NN), Parallelepiped (Para) and Spectral Angle Mapper (SAM). The results of the controlled classifications on the stacking of Landsat image bands from 2000 and 2020 were less consistent than those obtained with the index concatenation approach. The Para and DM classification algorithms were less efficient. With their respective Kappa scores ranging from 0.27 (2000 image) to 0.43 (2020 image) for Para and from 0.64 (2000 image) to 0.84 (2020 image) for DM. The results of the SAM classifier were satisfactory for the Kappa score of 0.83 (2000) and 0.88 (2020). The ML and NN were more suitable for the study area. Their respective Kappa scores ranged between 0.91 (image 2000) and 0.99 (image 2020) for the LM algorithm and between 0.95 (image 2000) and 0.96 (image 2020) for the NN algorithm.

Keywords: classification algorithms; methods evaluation; land cover change; mining locality

1. Introduction

Overall, primary tropical forests declined by 10% from 2021 to 2022 [1]. At the national level, the Democratic Republic of Congo (DRC) loses approximately 1.25 million hectares of its vegetation cover each year [2]. Rapid population growth in sub-Saharan Africa [3] and its corollaries are at the root of spatial changes [4,5] that can be characterized using remote sensing tools. This phenomenon is observed in all major cities and their surroundings in the DRC, where the population increased according to [6] from 30.7 million to 81.3 million between 1984 and 2017.

In the southeast of the country, mining activities promote the concentration of populations around countless copper (Cu) and cobalt (Co) mines, with the consequences of the anthropization of natural spaces [7]. Recent work by [8] on the assessment and mapping of deforestation in Katanga, by [9] which relates to the dynamics of Katanga forest ecosystems in the copper arc and the field observations carried out as part of this study, highlights significant environmental upheavals, which result from deforestation and anarchic mining. Khoji et al. [10] revealed that around Lubumbashi, Likasi, Fungurume and Kolwezi, the natural cover that dominated the landscape in 1979 lost more than 60% of its area in 41 years (1979–2020) to agricultural and energy production. This spatial dynamic was reported by [11]. Around Lubumbashi, 30 km from the Kipushi Mining Locality (LMK), between 1990 and 2022 approximately 40% of the Miombo forest was replaced by pasture [12].

The Kipushi Mining Locality (LMK), which became the rural commune of the same name, was born thanks to the development of the underground mine [13] of Zn, Cu and Lead (Pb) by the mining union of Haut-Katanga which later became the General Mines and Quarries (GCM). Since the fall of the latter in the 1990s, the population of this territory has resorted to agronomic practices, small cross-border trade, the exploitation of quarry materials and the collection of rocks containing Cu and Zn ores from the old backfill stored by the GCM. These activities have the consequences [14] of the restructuring of the spatial and landscape morphology in addition to [15,16] the fragmentation of natural landscapes that were already impacted by the activities of the CGM [17].

On the one hand, because of the expansion of human habitat both under the impetus of the LMK cores and the neighboring city of Lubumbashi. And on the other hand, the extension of agricultural areas [12], the increased collection of firewood, carbonization [18] and the exploitation of quarry materials from waste stored by the GCM. The movements of the latter reconfigure their footprints by modifying the landscape and land use. These claim the characterization of the change of spaces that it is important to capture, quantify and map in order to understand and evaluate the influence of human activities on the essential processes that govern the geosphere-biosphere system. And the remote sensing tool can precisely respond to this concern; but it is unclear which image classification or change detection method(s) would be appropriate for the heterogeneity of the study area.

The LMK has not benefited from studies on its land use dynamics at the scale of its territory. This foreshadowed the ignorance of the methods of remote sensing of change that would be relevantly applicable to our study environment. To ensure the robust extraction of information and their adequate groupings, before the multi-date comparison of the results. This reasoning was highlighted by several publications: 1) El Kharki et al. and N'guessan et al. [19,20] to evaluate the merits of the various methods of classification of satellite images; 2) Cabala et al. and André et al. [14,21] to quantify the anthropogenic effects or the dynamics of the landscape in the Lubumbashi plain; 3) Mas [22] to make the critical analysis of the main algorithms and techniques of remote sensing of change; 4) Nsiami [23] proposed the classification based on the textural analysis approach, considered suitable for mapping land use in a very heterogeneous urban environment.

Although remote sensing is emerging by democratizing data collection technologies and algorithms for extracting information contained in optical images, the choice of a method in this field remains judicious. This study aims to evaluate and compare two post-classification approaches to change detection, applied from independent classifications of Landsat images from 2000 and 2020. (1) Using supervised classification on images of colored compositions; (2) by exploiting the advanced classification method based on the technique of calculation and fusion of spectral indices (Normalized Difference Vegetation Index (NDVI), Normalized Difference Built-up Index (NDBI) and the Normalized Difference Water Index (NDWI)). In both cases, the research carried out a comparative evaluation of the performance of five variants of classifier algorithms, namely, Maximum likelihood, minimum distance, neural network, parallelepiped, and spectral angle mapper, to identify the tool adapted to the reality of the LMK environment.

The comparative study of performance was carried out on Landsat Thematic Mapper (TM), year 2000 and Enhanced Thematic Mapper Plus (ETM+) year 2020 images covering the LMK. Robustness tests were carried out on matrices of class separabilities and transitions whose statistical characteristics express the merit of each of the five methods evaluated.

2. Materials and methods

2.1. Study area

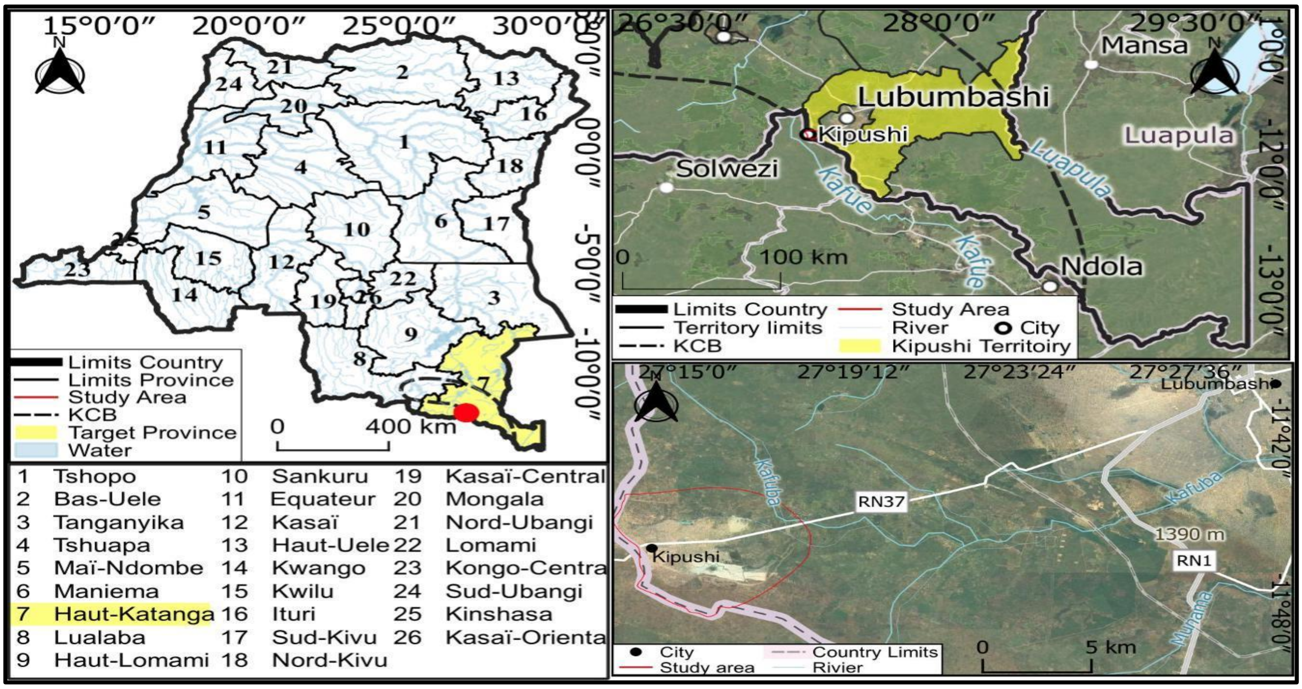

Figure 1. Study area.

The Kipushi Mining Locality (LMK) (became a rural commune about 10 years ago) has 38.95 km^2 and occupies ± 0.3% of the surface area of the territory of Kipushi in the south-east of the D.R. Congo, as shown in **Figure 1**. The diagonal coordinates: 27°13′26″ and 27°15′5″ East; −11°48′6″ and −11°44′27″ South, limit the study area with the city of Lubumbashi at the level of Mukulubwe stream to the north and the territory of Kasenga further; the terroir of Sakania to the south; the Republic of Zambia to the east and west. The north-western part of the research area shares the limits with the territory of Kambove and the Kaponda group via the Maimbudu River. Five districts: Kamarenge, Changalawe area, Chachacha GCM, Chachacha city and GCM Safricas installation—form the Kipishi in the Katangais CopperBelt (KCB), where mining operations and related activities are concentrated.

The LMK was separated from the city of Lubumbashi, located about 30 km away, by agricultural and forest areas. Some of these areas have undergone profound ecological transformations. Impacting the natural landscape which is deteriorating at a rate inversely proportional to the increase in human populations, highly dependent on natural resources and agriculture. In the region, the characterization of socio-ecological [24] MALAISSE and socio-economic [25] impacts of forests having been established, the situation of the spatio-temporal dynamics of occupation in the LMK would be less recorded due to the lack of specific studies.

2.2. Data and data sets

The study used multi-sensor optical images recorded respectively on the dates: (1) 10 August 2000; (2) 9 August 2020; in the same area (path: 173 and row: 068). Landsat 5 Thematic Mapper (TM) and Landsat 7 Enhanced Thematic Mapper Plus (ETM+) level 1, downloaded from the USGS Earth Explorer platforms. They all had the same spatial resolution of 30 m, suitable for spatial and temporal analysis of land cover changes between 2000 (LT05_L1TP_173068_20000810_20200907_02_T1) and 2020 (LE07_L1TP_173068_20200809_20200915_02_T1). The use of Landsat data for change detection is encouraged by several scientists: [26–28] because they offer long and continuous series of synoptic images.

Field data include direct observations and surveys of training areas. The Garmin Map 72 GPS with a precision of ± 3 m was used to locate the training areas, which facilitated the recognition of objects in the discrimination of land use classes according to their nomenclatures. Legacy data such as the plan of the city of Kipushi, developed by the Special Committee of Katanga (CSK) in 1957, the Shapefiles of administrative boundaries obtained from the open platform OpenStreetMap, supplemented the satellite images in the spirit of [29].

2.3. Image preprocessing

The quasi-permanent cloud cover in the tropical zone [30,31] radiation and others influence the shooting of optical images by introducing noise that could be reduced via atmospheric correction. Its application produced the complete radiometric calibration by standardizing the radiometric values between the two processed Landsat image scenes. This allowed the reproducibility of the analyses on multi-date images, covering the same geographical area studied. This calibration consisted of converting the pixel value (initially in relative luminance) into reflectance at the level of the atmosphere (TOA, for Top Of Atmosphere) from the sensor parameters and the spectral properties of the bands in the spirit of [32,33] by successively applying the two equations below:

1) Conversion to absolute luminance:

$$L = \mathrm{GAIN} \times \mathrm{DN} \times \mathrm{absacalfactor} \times \mathrm{effectivebandwidth} + \mathrm{OFFSET} \tag{1}$$

From where: DN is the digital count of the pixel; Gain is the gain for each spectral band, updated by DigitalGlobe; Offset is the offset for each spectral band, updated by DigitalGlobe; Abscalfactor is the calibration factor of the spectral band; Effective bandwith is the width of the spectral band.

2) Conversion to reflectance:

$$\rho(\text{TAO})_\lambda = \frac{L_\lambda d^2 \pi}{E_\lambda Cos\ \theta_s} \tag{2}$$

where: L_λ is the absolute luminance of the sensor for the spectral band λ expressed in W/m2/µm/sr; d is the Earth-Sun distance in astronomical units; E_λ is the exoatmospheric irradiance of the spectral band, in W/m^2/µm; and θ_s the solar zenith angle.

The Principal Components (PC) Spectral Sharpening model was applied to refine the spatial resolutions of multi-band images in order to benefit from the best 15 m resolution of the panchromatic band. This allowed us to resample the multispectral bands by changing them from 30 m to 15 m resolution. The Layer Stack files allowed us to act on all the bands targeted by the operation at the same time. This was followed by the extraction of the study area using the “Resize Data” algorithm. The reduction in the volume of information to be processed had the effect of optimizing the calculation time of the various parameters at the time of processing.

2.4. Processing

After the pre-processing, i.e., atmospheric and radiometric corrections and image cutting according to the limits of the study area, the calculations of the indices: Normalized Difference Vegetation Index (NDVI), Normalized Difference Built-up Index (NDBI) and Normalized Difference Water Index (NDWI) followed, which produced 3 neo-images that were combined to have a single image in colored composition. The layer stracking tool was used for this purpose by combining six bands (b): b1, b2, b3, b4, b5, b6 for the 2000 image and seven bands (b): b1, b2, b3, b4, b5, b6 and b7 for the 2020 image. It was possible to group the two images, respectively, from their metadata, then combine them with the neo-images.

Envi 5.1 software was used for remote sensing processing relating to the extraction and classification of information. And QGIS 3.4 facilitated the integration of data into a Geographic Information System (GIS) for further analysis and the edition of final maps of land use dynamics in the LMK.

2.4.1. Calculation of indices

The use of indices [34] to improve discrimination between classes is a common practice in remote sensing [35]. Thus, we calculated as shown in **Figure 2**, three spectral indices: Normalized Difference Vegetation Index (NDVI), Normalized Difference Built-up Index (NDBI) and Modified Normalized Difference Water Index (MNDWI), to simplify multi-temporal mapping of land use in the CRK. These indices, the most used to characterize vegetation [36], buildings [37], bare soils and wetlands, made it possible to synthesize and perform a binary reduction of a large volume of spectral information. This offered the study the possibility of discriminating classes based on a thresholding technique on a neo-image.

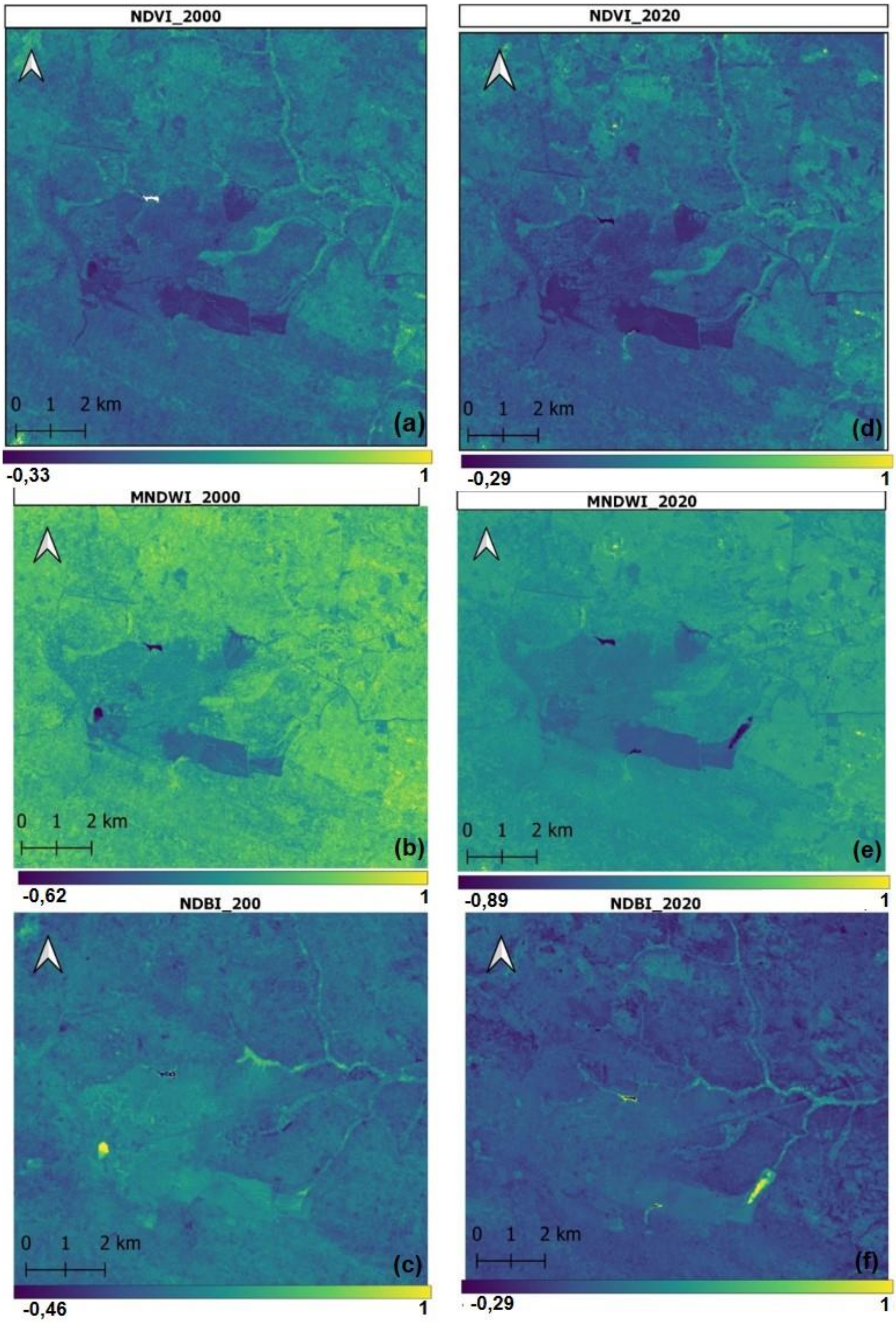

Figure 2. The indices: **(a)** and **(d)** NDVI; **(b)** and **(e)** MNDWI; and **(c)** and **(f)** NDBI, calculated on Landsat images from 2000 (left) and 2020 (right).

In different eco-geographic study contexts, Rouse JK et al. [38]; Bannari A et al. [39]; Yan Y et al. [40]; Le Gal A et al. [41] and Muhammad SR, Sarah S [42] calculated the NDVI by the following equation:

$$\mathrm{NDVI} = \frac{\mathrm{NIR} - \mathrm{Red}}{\mathrm{NIR} + \mathrm{Red}} \tag{3}$$

As for the calculation of NDBI, Doumit JAV, Sakr SC [35] and Zha Y, Gao J, Ni S. [43] propose the following formula:

$$\mathrm{NDBI} = \frac{\mathrm{SWIR1} - \mathrm{NIR}}{\mathrm{SWIR1} + \mathrm{NIR}} \tag{4}$$

The expression of MNDWI was proposed by [35,44] it is written:

$$\mathrm{MNDWI} = \frac{\mathrm{Green} - \mathrm{SWIR1}}{\mathrm{Green} + \mathrm{SWIR1}} \tag{5}$$

where, NIR stands for Near Infrared and SWIR stands for Short Wave Infrared.

2.4.2. Combination of special indices: NDVI, NDBI and MNDWI

In **Figure 3** we concatenated the indices using the sum and mean combination method, which are relatively simple to interpret and commonly used for various indices. The resulting distributions have the same form; only the scale is different. Therefore, the resulting index map has the same appearance. Only the values differ. This method allows high values in one variable to compensate for low values in another variable. This could avoid the problem of overestimating classes sensitive to one of the indices used, if it were exploited individually.

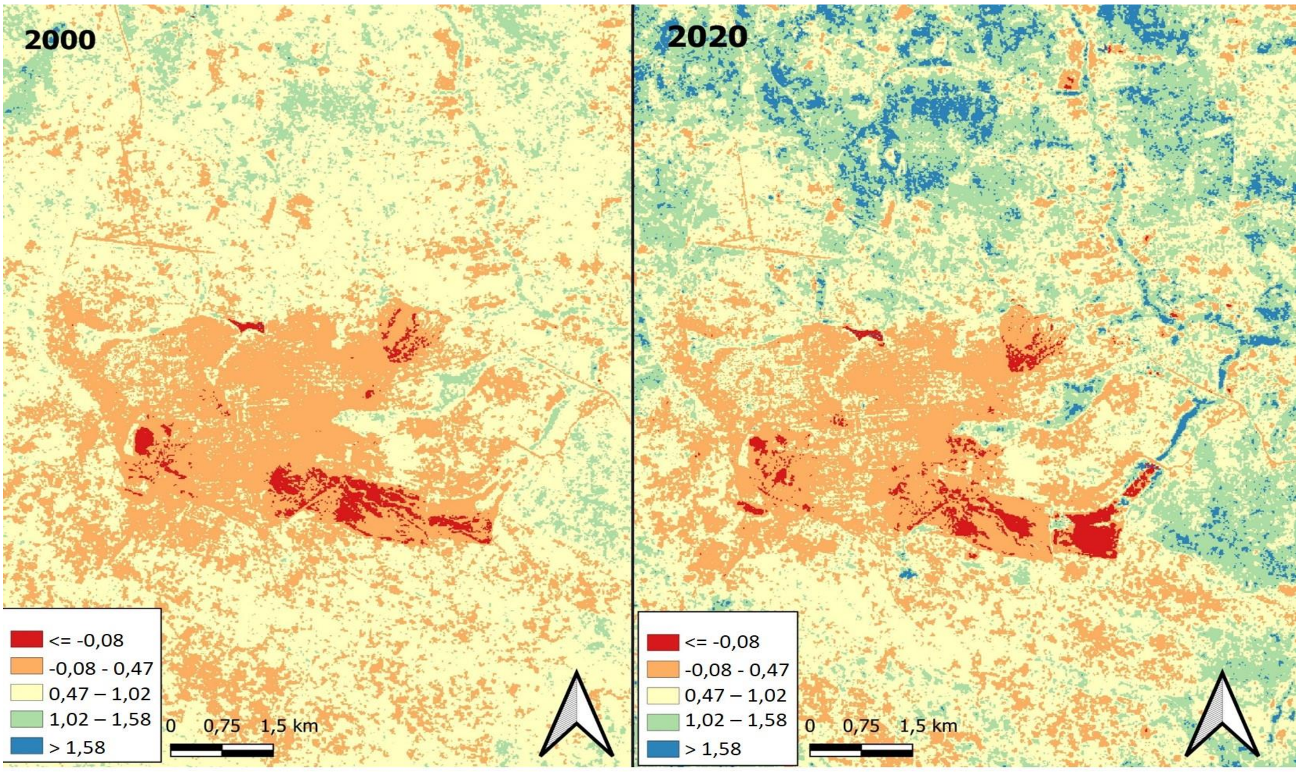

Figure 3. Normalized concatenation vegetation, water and built up indices (NCVWB) which vary between −2 and 2. In a 2000 (left) and 2020 (right) image before making classifications on them.

We had to impose the same class intervals for both maps to support the semantic value of the concatenation results. These intervals had the function of identifying the different land use classes by the technique of successive thresholdings. We approximately managed to characterize the classes by using just this concatenation of indices.

The classification technique based on a simple thresholding technique applied to a neo-image (index) has a weakness. That of statistical overestimation when discriminating classes from the group of objects with more sensitivity compared to the spectral bands involved in the mathematical calculation of this index. For example, the NDVI saturates when the vegetation cover is too important [45]. So, to get around this difficulty, the study used the index combination method: NDVI, NDBI and MNDWI, to respectively compose two multi-index neo-images from 2000 and 2020. On which we selected the training areas for assisted classifications using samples from the predefined classes.

2.4.3. Selection of training zones

The discrimination of degraded forests, less degraded forests, buildings, mine materials, bare soil and bodies of water was based on twelve training samples recorded in Shapefile format. Due to six classes (**Table 1** gives the descriptions) for each of the images from 2000 and 2020. The manual selection technique combined with photo-interpretation of the image was used to ensure the relative homogeneity of the sample sizes for each year considered. This step of major impact on the entire process of classifying an optical image led to the identification of two types of specimens. The first, known as training samples, covered on average 11.7% of processed images and were used in the classification calculation. The second type of samples consisted of 137 control points, surveyed with a pocket GPS, and made it possible to assess the quality of the classifications produced by the study.

Table 1. Categories land cover description.

Land cover	Number of pixels	Description
Waters and wetland	783	Vegetated lands with a high water table; standing water including rivers and water ponds.
Built-up	734	Residential land with minimal vegetation with impervious surfaces, constructed or paved roads.
Bare soil	775	Bare land with sparse vegetation, soil background and dirt roads.
Mine materials	689	Bare land with sparse vegetation, soil background and dirt roads.
Degraded forest	817	Woody vegetation cover is dominated by shrub species with interspersed savannas and meadows. It is distinguished from less degraded forest by the low density or abundance of the tree layer and the height of the trees. It contains trees and herbaceous vegetation.
Less degraded forest	762	Mosaic of several types of forests: Dry and riparian evergreen forests, dominated by Miombo. Plant formations with more or less closed stands. Riparian evergreen forests include forest ecosystems that colonize along rivers and islets, and thus benefit from particular soil conditions in areas characterized by a long dry season. Miombo forest is a type of vegetation, dominant in the Zambezian region, characterized by the predominance of species belonging to the genera Brachystegia, Julbernardia and Isoberlinia.

2.4.4. Image classification from 2000 and 2020

Remote sensing is increasingly democratizing data collection technologies and enhancing the accessibility of algorithms for extracting information from optical imagery. However, selecting an appropriate method remains a critical step in ensuring reliable results. This study evaluated and compared two post-classification approaches for land use and land cover change detection, applied to independently classified Landsat images from 2000 and 2020.

1) Supervised classification of multispectral imagery

This approach involved the classification of color composite images using supervised learning techniques.

2) Advanced classification based on spectral index fusion

This method utilized the calculation and combination of multiple spectral indices, namely the Normalized Difference Vegetation Index (NDVI), Normalized Difference Built-up Index (NDBI), and Modified Normalized Difference Water Index (MNDWI), to enhance class separability and reduce classification errors related to interclass confusion.

In both approaches, the classification accuracy was assessed by comparing the performance of five supervised machine-learning classifiers (see **Table 2**):

- Maximum Likelihood Classifier (MLC): A probabilistic classifier based on Bayesian decision theory that assumes normal distribution for each class and calculates the probability of a pixel belonging to a given class.
- Minimum Distance Classifier (MDC): A simple algorithm that assigns a pixel to the class whose mean spectral signature is closest in feature space.
- Artificial Neural Network (ANN): A machine learning model that learns complex patterns in spectral data through a system of interconnected neurons, optimizing classification based on training data.
- Parallelepiped Classifier: A rule-based classification technique that assigns pixels to classes based on predefined spectral range thresholds for each band.
- Spectral Angle Mapper (SAM): A physically-based classifier that calculates the spectral angle between the pixel's reflectance spectrum and reference spectra, assigning the pixel to the class with the smallest angle.

These algorithms were trained using region of interest (ROI) samples collected from the images. Training samples were selected through a stratified random sampling approach to ensure representative coverage of different land cover types. The classification was then applied separately to two Landsat scenes (2000 and 2020), with accuracy evaluated on a pixel-by-pixel basis. The post-classification change detection was conducted using a change matrix, comparing land cover transitions between the two years.

Since classification accuracy is a crucial factor in change detection, particular attention was given to the impact of spectral index fusion. The classification approach based on spectral index fusion aimed to minimize the overestimation of interclass changes commonly observed in conventional classification techniques [22].

Table 2. Classification scores with different algorithms used.

Classification with the maximum likelihood algorithm (LM)		
Year	2000	2020
Overall Accuracy (%)	92.75	99.11
Kappa (%)	0.91	0.99
Classification with the Minimum Distance algorithm (DM)		
Year	2000	2020
Overall Accuracy (%)	71.33	87.26
Kappa (%)	0.64	0.84
Classification with Neural Network algorithm (NN)		
Year	2000	2020
Overall Accuracy (%)	95.43	95.43
Kappa (%)	0.95	0.96
Classification with the Parallepiped algorithm (Para)		
Year	2000	2020
Overall Accuracy (%)	24.93	32.83
Kappa (%)	0.27	0.43
Classification with the Spectral Angle Mapper algorithm (SAM)		
Year	2000	2020
Overall Accuracy (%)	87.12	90.30
Kappa (%)	0.83	0.88

In order to characterize the dynamics of land use in the rural commune of Kipushi, we have at this stage assigned a specific class to each pixel. The classifications integrated the pixels according to their attributes by linking them to an object (region of interest: ROI). The assignment of a pixel was based on the resemblance between the spectral signature of the pixel and the spectral signature of the class according to the prescription of [46].

2.4.5. Change detection

The highlighting of the human impact on the change of land use in the area was obtained using the transition matrix created to identify the transition frequencies between land use classes over the time interval studied [47]. This matrix is obtained by crossing the land use maps of two comparative periods (2000 and 2020). Indeed, the transition matrix is one of the main models for assessing landscape changes [47]. It is a graph showing the transitions between classes over a given period, therefore the transition percentages observed over a specific time [11].

In this study, the comparative transition matrices were developed in post-classification processing after classification with the algorithms of Maximum likelihood, minimum distance, neural network, parallelepiped, and spectral angle mapper. **Table 3** compares their performances via the analysis of Landsat TM (2000) and ETM+ (2020) images covering the CRK.

Table 3. Accuracy assessment and area estimate for land cover and land cover change maps from 2000 to 2020.

2000–2020	Waters and wetlands	Built-up	Bare soil	Mine materials	Degraded forest	Less degraded forest
Accuracy measure						
Prod. acc.	78.51%	40.58%	48.55%	42.83%	85.73%	55.62%
User acc.	100%	100%	100%	100%	100%	100%
Overall acc.	95.43%					
Stratified estimators of area ± CI [% of total map area]						
Area	21.49%	59.42%	51.45%	57.17%	14.23%	44.38%
95% CI	−13.8%	6.88%	83.43%	−47.77%	3.96%	−15.51%

Robustness tests were carried out on matrices of class separabilities and transitions whose statistical characteristics express the merit of each of the five methods evaluated.

3. Results and discussion

3.1. Land cover mapping

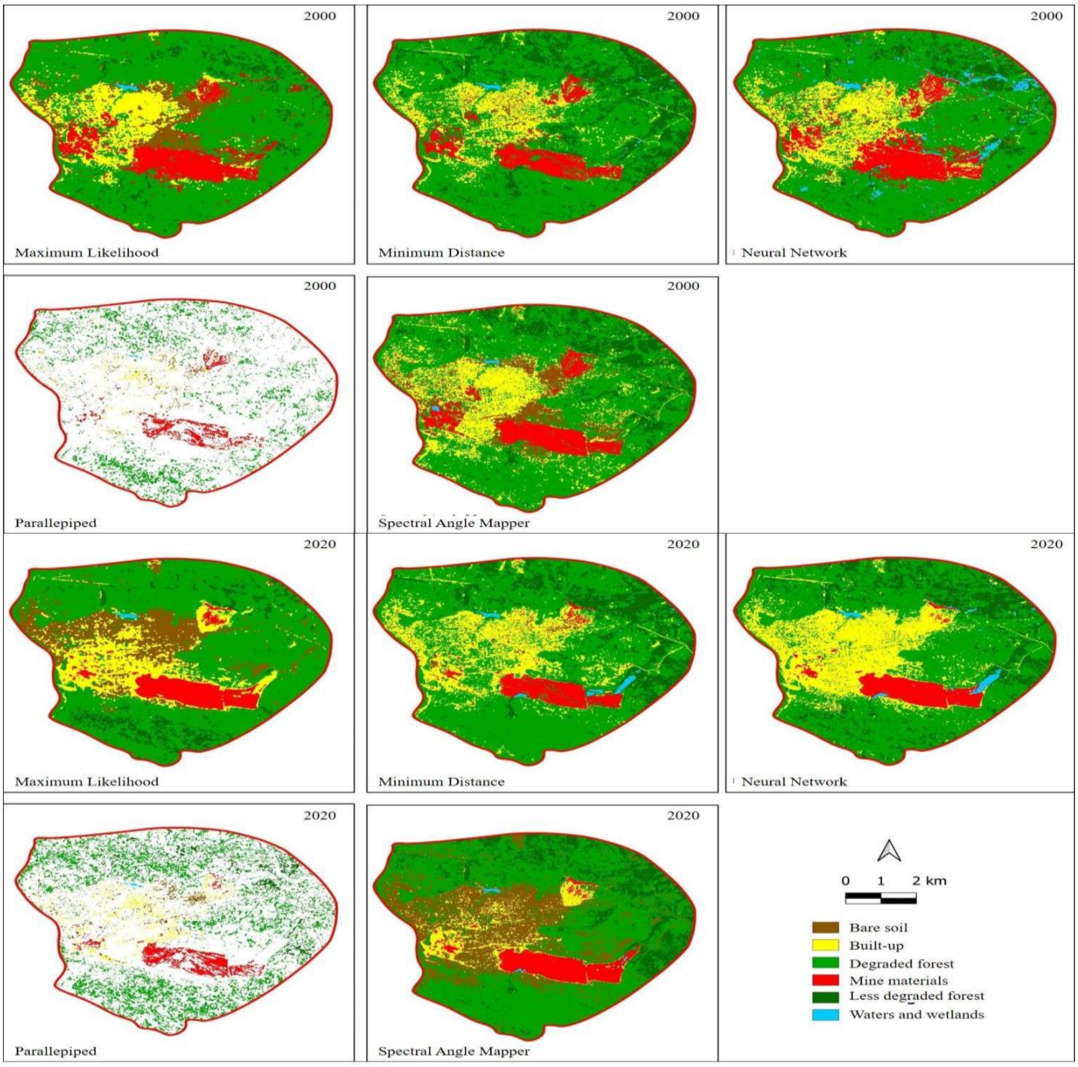

Figure 4. Classification from the methods evaluated for the years 2000 and 2020.

This study produced ten land cover maps from these analyses based on five classification algorithms. The interpretation based on visual analysis of the results revealed that each of the six land cover classes assessed presents either a regressive trend or a progressive trend in terms of spatiotemporal dynamics. In detail, the change matrix recorded a decrease in less degraded forest cover in 2020 compared to 2000. Indeed, the large forest areas that dominated the landscape of the Kipushi mining locality (LMK) in 2000 have been replaced by bare soil, buildings and degraded forests (**Figure 4**).

3.2. Land cover composition based on results: LM, DM, NN, Para and SAM

The evaluation of the five classification methods, namely, Maximum Likelihood (ML), Minimum Distance (MD), Neural Network (NN), Parallelepiped (Para) and Spectral Angle Map (SAM), shows that the Para and DM classification algorithms were less efficient. With their respective Kappa scores ranging between 0.27 (image 2000) and 0.43 (image 2020) for Para and between 0.64 (image 2000) and 0.84 (image 2020) for DM. The results from the SAM classifier were satisfactory for the Kappa score of 0.83 (2000) and 0.88 (2020). The ML and NN were more suitable for the study area. Their respective Kappa scores had varied between 0.91 (image 2000) and 0.99 (image 2020) for the LM and between 0.95 (image 2000) and 0.96 (image 2020) for the NN algorithm. As we could read via **Table 2**, their performances were better compared to those shown by the Kappa scores obtained with the three other methods: Para, DM and SAM.

3.3. Land cover transfers between 2000 and 2020

In the study area, degraded forest was found to be the most stable land use class between 2000 and 2020 (**Table 3**). The built-up area class comes second with a stability of around 7%. Furthermore, the remarkable dynamics of the bare soil class emerged in the landscape, particularly at the expense of less degraded forest (−15.51%), water and wetlands (−13.8%) and bare soil (83%). wooded savannah (3.1%) and grassy savannah (1.0%). In the interval of the study period, 60% of the quarry and mining materials occupation class evolved towards bare soil (55%) and built-up soil (5%). Between 2000 and 2020, the other classes (Waters and wetlands, bare soil, less degraded forest) of the mining locality of Kipushi decreased in favor of Built-up; in variable extents (2.5% to 17.6%). **Table 4** below provides a summary of the changes that each of the occupation classes had recorded in 20 years.

Table 4. Estimation of land use conversions between 2000 and 2020 in the mining town of Kipushi.

2000–2020	Waters and wetlands	Built-up	Bare soil	Mine materials	Degraded forest	Less degraded forest
95% CI	−13.8%	6.88%	83.43%	−47.77%	3.96%	−15.51%

3.4. Dynamics of spatial changes

Table 5. Transition probability matrix (as a percentage of class area) illustrating the conversion of land use class areas between 2000 and 2020 in the Kipushi mining town. The stability of the land use area is illustrated by the bold values.

LM 2000–2020	**Waters and wetlands**	**Built-up**	**Bare soil**	**Mine materials**	**Degraded forest**	**Less degraded forest**		
Waters and wetlands	**13.60**	0.18	0.00	0.01	0.42	0.20		
Built-up	0	**2.85**	1.59	0.15	0.15	0.00		
Bare soil	0.00	0.76	**5.30**	0.15	0.13	0.00		
Mine materials	0.00	0.99	0.59	**20.36**	0.09	0.00		
Degraded forest	0.14	1.11	2.94	0.11	**17.10**	6.95		
Less degraded forest	0.00	0.03	0.06	0.01	13.81	**10.20**		
Total	13.74	5.92	10.49	20.78	31.71	17.36	100.00	
DM 2000–2020	Waters and wetlands	Built-up	Bare soil	Mine materials	Degraded forest	Less degraded forest		
Waters and wetlands	**15.90**	0.00	0.00	0.00	0.13	0.01		
Built-up	0.00	**8.30**	0.10	0.01	0.00	0.04		
Bare soil	0.00	0.07	**14.20**	0.21	0.00	0.00		
Mine materials	0.00	0.63	0.17	**26.50**	0.00	0.00		
Degraded forest	0.08	0.79	0.00	0.03	**12.20**	2.34		
Less degraded forest	0.10	0.00	0.00	0.00	8.80	**9.39**		
Total	16.07	9.79	14.47	26.75	21.13	11.78	100.00	
NN 2000–2020	Waters and wetlands	Built-up	Bare soil	Mine materials	Degraded forest	Less degraded forest		
Waters and wetlands	**14.10**	0.00	0.00	0.00	1.17	1.29		
Built-up	0.00	**3.45**	0.01	0.13	0.02	0.00		
Bare soil	0.00	0.22	**8.60**	0.00	0.21	0.00		
Mine materials	0.03	1.51	0.00	**25.70**	0.50	0.00		
Degraded forest	0.09	0.75	0.00	0.01	**17.10**	10.44		
Less degraded forest	0.01	0.04	0.00	0.00	1.30	**13.30**		
Total	14.24	5.97	8.61	25.84	20.31	25.04	100.00	
Para 2000–2020	Waters and wetlands	Built-up	Bare soil	Mine materials	Degraded forest	Less degraded forest	Unclassified	
Waters and wetlands	**11.50**	0.00	0.00	0.00	0.00	0.00	0.00	
Built-up	0.00	**4.00**	0.01	0.00	0.00	0.00	0.00	
Bare soil	0.00	0.01	**6.80**	0.00	0.00	0.00	0.00	
Mine materials	0.00	0.00	0.00	**12.60**	0.00	0.00	0.00	
Degraded forest	0.00	0.00	0.00	0.00	**15.82**	0.00	0.00	
Less degraded forest	0.00	0.00	0.00	0.00	0.00	**13.01**	0.00	
Unclassified	0.03	0.13	0.08	0.30	7.94	7.91	**19.85**	
Total	11.53	4.14	6.89	12.90	23.76	20.92	19.85	100.00

Table 5. (*Continued*).

SAM 2000–2020	Waters and wetlands	Built-up	Bare soil	Mine materials	Degraded forest	Less degraded forest	
Waters and wetlands	**12.30**	0.02	0.00	0.00	0.00	0.00	
Built-up	0.00	**5.24**	4.79	0.05	0.53	0.00	
Bare soil	0.00	0.65	**7.54**	0.24	0.05	0.00	
Mine materials	0.00	0.48	0.03	**23.78**	0.00	0.00	
Degraded forest	0.02	0.01	0.51	0.08	**18.68**	8.18	
Less degraded forest	0.00	0.00	0.00	0.00	4.31	**12.50**	
Total	12.33	6.41	12.87	24.15	23.56	20.68	100.00

The analysis and interpretation of **Table 5** highlight two major phenomena: Attrition and aggregation; which have affected, with varying intensities, the land use classes of the mining locality of Kipushi (LMK). On the one hand, the respective regressions of the classes: Water and wetlands, Mining materials and less degraded forest could be explained by the predominance of the fragmentation process of the blocks (plots) constituting the previously mentioned classes. The class of mining and quarry materials formerly stored in the form of backfill was striking in the landscape of the LMK. Its dynamics in the Katanga CopperBelt could be explained by the anthropic-geomorphological mutations studied by [47]. On the other hand, the bare soil, the degraded forest and the Built which have spatially conquered spaces would have undergone the phenomenon of aggregation; since we observed decreases in the spatial dispersions of the pixels constituting these last three classes in favor of the increase in their areas marked by the gain in occupied areas.

4. Discussion

Many studies: [8–12,14,22] etc. have addressed the problem of detecting land use changes in the Lubumbashi region and its surroundings, but they have not explored the technique of concatenation of spectral indices (NDVI, NDBI and NDWI), nor addressed the problem of evaluating classification methods, evaluated in this manuscript. Research similar to ours has been conducted by [43,48] for the delimitation of urban areas or for the detection of land use changes [49] from a Landsat image. Their studies had valued the NDBI or the NDVI and the NDWI and without favoring the technique of concatenation of three indices (NDVI, NDBI and NDWI) used by the present study. This is highlighted by the divergence of our respective results. For example, Zha Y, Gao J, Ni S. [43] achieved an overall accuracy of 39.82% with the NN algorithm in mapping urban areas of Nanjing city in southeast China.

The NN method finds pixel clusters in spectral terms and not in thematic terms. Unlike the SAM approach frequently used in spatiotemporal assessment of urban extensions [50]. Its advantage is that it assigns each pixel in the image to a class by comparing it to reference samples [51]. In this way, the success of remote sensing image classification will depend on many factors such as the availability of high-quality remote images and auxiliary data, the design of a procedure, the choice of an appropriate classification method, and the skill and experience of the analyst [52].

5. Conclusion

The study aimed to evaluate five classification algorithms: (1) Maximum likelihood (ML); (2) minimum distance (MD); (3) neural network (NN); (4) parallelepiped (Para); and (5) spectral angle mapper (SAM). To identify which of these five methods would be suitable for mapping land use dynamics in the mining city of Kipushi. This evaluation proceeded by supervised classifications on Landsat optical images and on the concatenation products of neoimages from 2000 and 2020, resulting from the combination of spectral indices: NDVI, NDBI and NDWI; finally to search for the robust tool for extracting the information contained in the images and their adequate groupings, before the multi-date comparison of the results.

The results of the land use mapping obtained in this study showed that each of the six land use classes assessed presents either a regressive trend or a progressive trend in terms of spatiotemporal dynamics. In detail, the change matrix recorded a decrease in less degraded forest cover in 2020 compared to 2000. Indeed, the large forest areas that dominated the landscape of the Kipushi mining town in 2000 have been replaced by bare soil, buildings and degraded forests.

It was found that among the five classification methods (LM, DM, NN, Para and SAM) the Para and DM classification algorithms were less efficient. Their respective Kappa scores ranged between 0.27 (2000 image) and 0.43 (2020 image) for Para and between 0.64 (2000 image) and 0.84 (2020 image) for DM. While the results from the SAM classifier were satisfactory with the Kappa score of 0.83 (2000) and 0.88 (2020). The LM and the NN were more suitable for the study area. Their respective Kappa scores had varied between 0.91 (image 2000) and 0.99 (image 2020) for the LM and between 0.95 (image 2000) and 0.96 (image 2020) for the NN algorithm. Their performances were better compared to those shown by the Kappa scores obtained with the other three methods: Para, DM and SAM.

The results presented in this work are focused on traditional algorithms. Future research should look at the concatenation of land use indices applied in machine learning and deep learning in heterogeneous mining environments to test the robustness of existing models.

Author contributions: Conceptualization, ONI and YKL; methodology, UKT; software, UKT; validation, JMM (Joseph Mukalay Muamba) and CNM; formal analysis, ONI, JTWI and YKL; investigation, ONI, JTWI and YKL; resources, JMM; data curation, JTWI; writing—original draft preparation, JMM (Junior Muyumba Munganga); writing—review and editing, JTWI; visualization, ONI, JTWI and YKL; supervision, JMM (Joseph Mukalay Muamba) and CNM; project administration, JTWI; funding acquisition, JTWI. All authors have read and agreed to the published version of the manuscript.

Institutional review board statement: Not applicable.

Informed consent statement: Not applicable.

Conflict of interest: The authors declare no conflict of interest.

References

1. Mikaela W, Elizabeth G, Sarah C. How much forest was lost in 2022? Available online: https://research.wri.org/gfr/global-tree-cover-loss-data-2022 (accessed on 15 December 2024).
2. FAO. Global Forest Resources Assessment. Report Democratic Republic of the Congo. 2020.
3. Tabutin D, Schoumaker B. Demographics in Sub-Saharan Africa in the 21st Century: Taking Stock of Changes from 2000 to 2020, Prospects and Challenges to 2050 (French). Population. 2020; 75(2): 169–295. doi: 10.3917/popu.2002.0169
4. Delaunay D, Guengant JP. The Demographic Dividend in Sub-Saharan Africa (French). Monographies Sud-Nord. 2019.
5. Magrin G, Ninot O. Transitions and development in Africa: A continent of uncertainty. Bulletin de l'Association de géographes français. 2021; 97(4): 395–411. doi: 10.4000/bagf.7168
6. Pourtier R. The Democratic Republic of Congo faces the democratic challenge (French). Available online: https://www.ifri.org/sites/default/files/migrated_files/documents/atoms/files/pourtier_rdc_defi_demographique_2018.pdf (accessed on 15 December 2024).
7. Amisi M. The perception of the impact of mining activities in Katanga: Analysis by applying Kevin Lynch's landscape theory [PhD thesis]. Department of Geography, Faculty of Sciences, University of Lubumbashi; 2010. pp. 254–257.
8. Kabulu Djibu JP. Evaluation and mapping of deforestation in Katanga [DEA thesis in geographical sciences]. Free University of Brussels; 2006.
9. Cabala Kaleba S, Useni Sikuzani Y, Sambieni KR, et al. Dynamics of Katangese forest ecosystems in the copper arc in the Democratic Republic of Congo: I. Causes, spatial transformations and magnitude. Tropicultura. 2017; 35 (3): 192–202.
10. Muteya HK, Nghonda DDN, Malaisse F, et al. Quantification and Simulation of Landscape Anthropization around the Mining Agglomerations of Southeastern Katanga (DR Congo) between 1979 and 2090. Land. 2022; 11(6): 850. doi: 10.3390/land11060850
11. Sikuzani YU, Muteya HK, Bogaert J. Miombo woodland, an ecosystem at risk of disappearance in the Lufira Biosphere Reserve (Upper Katanga, DR Congo)? A 39-years analysis based on Landsat images. Global Ecology and Conservation. 2020; 24: e01333. doi: 10.1016/j.gecco.2020.e01333
12. Muteya HK, N'Tambwe Nghonda DD, Kalenda FM, et al. Mapping and Quantification of Miombo Deforestation in the Lubumbashi Charcoal Production Basin (DR Congo): Spatial Extent and Changes between 1990 and 2022. Land. 2023; 12(10): 1852. doi: 10.3390/land12101852
13. De Vos W, Viaene W, Moreau J, Wautier J. Mineralogy of the Kipushi deposit, Shaba, Zaire. Centre of the Geological Society of Belgium, stratiform deposit and copper provinces, Liège. 1974; 165–183.
14. Sylvestre CK, Yannick US, François MK, Jan B. Anthropogenic activities and spatiotemporal dynamics of the open forest in the Lubumbashi Plain (French). In: Bogaert J, Colinet G, Mahy G (editors). Anthropisation of Katangan landscapes. Presses Universitaires de Liège; 2018. pp. 253–266.
15. Malaisse F, Colonval-Elenkov E, Brooks RR. The impact of copper and cobalt orebodies upon the evolution of some plant species from Upper Shaba, Zaire. Plant Systematics and Evolution. 1983; 142(3–4): 207–221. doi: 10.1007/bf00985899
16. Binzangi Kamalandua K, Tshibangu K, Malaisse F. Deforestation in tropical Africa. Défis-Sud. 1994; 36–37.
17. Amisi YM, Vranken I, Nkulu J, et al. Mining activity in Katanga and the perception of its impacts in Lubumbashi, Kolwezi, Likasi and Kipushi. In: Bogaet J, Colinet G, Mahy G (editors). Anthropization of Katangan landscapes. Presses universitaires d Liège; 2018. pp. 267–279.
18. Djibu Kabulu JP, Vranken I, Bastin JF, et al. Charcoal supply to Lushu households: Quantities, alternatives and consequences. In: Bogaert J, Colinet G, Mahy G (editors). Anthropization of Katanga landscapes. Presses Universitaires de Liège; 2018. pp. 297–311.
19. El Kharki O, Mechbouh J, Rouchdi M, et al. The effects of the scale level and of the spatial resolution on the object oriented classification: Application to mapping Arganeraie (region Agadir, Morocco). International Journal of Innovation and Scientific Research. 2015; 14(1): 21–31.
20. Akoguhi PN, Dibi HN, Godo MH, et al. Evaluation of directed classification methods (spectral and object-oriented) on THRS satellite images: Case of urban fabric mapping of the commune of Cocody and Attécoubé (Abidjan, Ivory Coast) (French). VertigO. 2022; 22(3): 1–32. doi: 10.4000/vertigo.36548
21. André M, Vranken I, Boisson S, et al. Quantification of anthropogenic effects in the landscape of Lubumbashi. In: Bogaert J, Collinet G, Mahy G (editors). Anthropisation des paysages katangais. Presses Universitaires de Liège; 2018. pp. 231–251.

22. Mas JF. A review of methods and techniques for remote sensing of change (French). Canadian Journal of Remote Sensing. 2000; 26(4): 349–362. doi: 10.1080/07038992.2000.10874785
23. Nsiami MC. Textural analysis of the Quickbird panchromatic image at very high spatial resolution: Application to the differentiation of land use types in Lubumbashi [PhD thesis]. University of Lubumbashi; 2009.
24. Malaisse F. Feeding in African open forest: Ecological and nutritional approach. Available online: https://cgspace.cgiar.org/bitstream/10568/64509/1/846_Black_and_White_Se_nourir_en_foret_claire_africaine.pdf (accessed on 13 September, 2022).
25. UN-REDD. Qualitative studies on the causes of deforestation and forest degradation in the Democratic Republic of Congo (French). Available online: https://www.forestcarbonpartnership.org/sites/fcp/files/2015/March/12-08-08%20PI%20Causes%20Etude%20qualitative%20causes%20DD%20PNUE.pdf (accessed 8 January 2025).
26. Wulder MA, Hermosilla T, White JC, et al. Augmenting Landsat time series with Harmonized Landsat Sentinel-2 data products: Assessment of spectral correspondence. Science of Remote Sensing. 2021; 4: 100031. doi: 10.1016/j.srs.2021.100031
27. Chatterjee U, Majumdar S. Impact of land use change and rapid urbanization on urban heat island in Kolkata city: A remote sensing based perspective. Journal of Urban Management. 2022; 11(1): 59–71. doi: 10.1016/j.jum.2021.09.002
28. Nazombe K, Nambazo O. Monitoring and assessment of urban green space loss and fragmentation using remote sensing data in the four cities of Malawi from 1986 to 2021. Scientific African. 2023; 20: e01639. doi: 10.1016/j.sciaf.2023.e01639
29. Ding Q, Shao Z, Huang X, et al. Time-series land cover mapping and urban expansion analysis using OpenStreetMap data and remote sensing big data: A case study of Guangdong-Hong Kong-Macao Greater Bay Area, China. International Journal of Applied Earth Observation and Geoinformation. 2022; 113: 103001. doi: 10.1016/j.jag.2022.103001
30. Tonye E, Akono A, Ndi Nyoungi A, Assako RJ. Use of ERS-1 and SPOT data for monitoring peripheral growth in the city of Yaoundé (Cameroon). In: Bannari A (editor). Optical and radar remote sensing and geomatics for the management of environmental problems. University of Ottawa; 1999. pp. 83–98.
31. Mouafo D. Geographic information systems, urban planning and development in Africa: Evolution, challenges and perspectives. International Journal of Geomatics. 2000; 213–239.
32. Schowengerdt RA. In: Remote Sensing: Models and methods for image processing, 3rd ed. Elsevier; 2007. pp.1–44.
33. USGS. Landsat Missions: Using the USGS Landsat Level-1 Data Product. Available online: https://www.usgs.gov/landsat-missions/using-usgs-landsat-level-1-data-product#web-tools (accessed 8 January 2025).
34. Pelletier C. Land use mapping from high-resolution satellite image time series [PhD thesis]. University of Toulouse; 2017. pp. 289.
35. Doumit JAV, Sakr SC. Mapping bare soil in the Bekaa Valley using remote sensing (French). InterCarto InterGIS. 2015; 1(21): 19–24. doi: 10.24057/2414-9179-2015-1-21-19-24
36. Spadoni GL, Cavalli A, Congedo L, Munafò M. Analysis of Normalized Difference Vegetation Index (NDVI) multi-temporal series for the production of forest cartography. Remote Sensing Applications: Society and Environment. 2020; 20: 100419. doi: 10.1016/j.rsase.2020.100419
37. Hassani N, Lebaut S, Sghir S, Drogue G. Evaluation of the impact on surface temperature of some emblematic redevelopment projects in the metropolitan area of Casablanca (Morocco). In: Proceedings of the 34th Annual Symposium of the International Climatological Association; 7 to 8 July 2021; Casablanca, Morocco.
38. Rouse JK, Haas RH, Schell JA, Deering DW. Monitoring vegetation systems in the Great Plains whith ERTS. Environmental Science. 1974; 309–317.
39. Bannari A, Morin D, Bonn F, Huete AR. A review of vegetation indices. Remote Sensing Reviews. 1995; 13(1–2): 95–120. doi: 10.1080/02757259509532298
40. Yan Y, Mao K, Shen X, et al. Evaluation of the influence of ENSO on tropical vegetation in long time series using a new indicator. Ecological Indicators. 2021; 129: 107872. doi: 10.1016/j.ecolind.2021.107872
41. Le Gal A. Multi-temporal study of the evolution of pyroclastic deposits and lahars deposited in the watershed most impacted by the eruption of Merapi in 2010 using very high resolution images. Engineering Sciences [physics]. 2018.
42. Muhammad SR, Sarah S. Landsat satellite imagery for analysis of terrestrial vegetation using NDVI method in Indonesian soil from 2014 to 2024. Journal of Geosciences and Geophysics. 2024; 12(3): 350–357.
43. Zha Y, Gao J, Ni S. Use of normalized difference built-up index in automatically mapping urban areas from TM imagery. International Journal of Remote Sensing. 2003; 24(3): 583–594. doi: 10.1080/01431160304987

44. McFeeters SK. The use of the Normalized Difference Water Index (NDWI) in the delineation of open water features. International Journal of Remote Sensing. 1996; 17(7): 1425–1432. doi: 10.1080/01431169608948714
45. Alexander. Precision agriculture: What is the NDVI index. Available online: https://farmonaut.com/remote-sensing/ndvi-explained-what-is-ndvi-index-and-how-it-revolutionizes-precision-agriculture/ (accessed on 4 November 2024).
46. Barima YSS, Barbier N, Bamba I, et al. Landscape dynamics in the Ivorian forest-savanna transition environment (French). Bois & Forets Des Tropiques. 2009; 299(299): 15. doi: 10.19182/bft2009.299.a20419
47. Tshibangu WIJ, Kalombo DK, Inabanza ON, et al. Contributions of Remote Sensing and GIS to the Inventory and Mapping of Colonial Geodetic Markers in the Katangese Copper Belt. Revue Internationale de Géomatique. 2024; 33(1): 15–35. doi: 10.32604/rig.2024.046629
48. Cabral P. Delimitation of urban areas from a Landsat ETM+ image: Comparison of classification methods (French). Canadian Journal of Remote Sensing. 2007; 33(5): 422–430. doi: 10.5589/m07-039
49. Dourado GF, Motta JS, Filho ACP, et al. The Use of Remote Sensing Indices for Land Cover Change Detection. Anuário do Instituto de Geociências—UFRJ. 2019; 42(2): 72–85.
50. Kieffer E, Serradj A. Remote sensing for urban studies: Expansion of the city of Pondicherry between 1973 and 2009 (French). Géomatique Expert. 2013; 68–79.
51. Duarte A, Codevilla F, Gaya JDO, da Costa Botelho SS. A dataset to evaluate underwater image restoration methods. OCEANS 2016—Shanghai. 2016; 1–6. doi: 10.1109/oceansap.2016.7485524
52. Aldoski J, Mansor SB, Shafri H, Shafri M. Change Detection Processes and Techniques. Civil and Environmental Research. 2013; 3(10): 37–45